

Cellular flow control design for mixing based on the least action principle

Weiwei Hu* Ming-Jun Lai† Hao-Ning Wu‡

October 28, 2025

Abstract

We consider a novel approach for the enhancement of fluid mixing via pure stirring strategies building upon the Least Action Principle (LAP) for incompressible flows. The LAP is formally analogous to the Benamou–Brenier formulation of optimal transport, but imposes an incompressibility constraint. Our objective is to find a velocity field, generated by Hamiltonian flows, that minimizes the kinetic energy while ensuring that the initial scalar distribution reaches a prescribed degree of mixedness by a finite time. This formulation leads to a “point to set” type of optimization problem which relaxes the requirement on controllability of the system compared to the classic LAP framework. In particular, we assume that the velocity field is induced by a finite set of cellular flows that can be controlled in time. We justify the feasibility of this constraint set and leverage Benamou–Brenier’s results to establish the existence of a global optimal solution. Finally, we derive the corresponding optimality conditions for solving the optimal time control and conduct numerical experiments demonstrating the effectiveness of our control design.

Keywords. Fluid mixing, least action principle, optimal transport, cellular flows, point to set optimization

1 Introduction

This work is concerned with the bilinear control of fluid mixing via two-dimensional cellular flows based on the Least Action Principle (LAP) for incompressible flows (e.g. [1, 2]). Fluid mixing, the process of dispersing one material or field in another medium, is fundamental to both natural phenomena and industrial applications, from atmospheric dynamics [3] to microfluidic devices [4]. It is governed by two primary mechanisms: *advection*, the transport by a fluid’s bulk motion, and *diffusion*, the spreading due to molecular motion. This study focuses on advection dominant regimes, characterized by a high Péclet number, where rapid flow transport renders diffusion negligible. Such conditions are typical in systems with high velocities, large length scales, or significant turbulence, where advective time scales are markedly shorter than diffusive ones, and hence effectively reduce the system dynamics to those of pure transport. In these regimes, mixing is governed solely by advection. We accordingly address the problem of optimal mixing of through stirring or active control of flow advection. In particular, the laminar advection is at core of our investigation, where a deterministic flow is introduced.

Stirring strategies for purely advective systems have been extensively studied in the literature. As explored in the pioneering work [5] by Aref, mixing can be achieved by inducing chaotic advection in laminar flows through a simple and regular flow field. In other words, complex particle trajectories can be generated by deterministic velocity fields. This phenomenon provided a mechanism for efficient fluid stretching and folding without turbulence and it was formalized in the kinematic framework in [6] by Ottino. A common approach for optimal stirring is to formulate an optimization problem for finding an optimal velocity field or a related protocol that enhances mixing under constraints such as fixed energy, enstrophy, or action (e.g. [7, 8, 9, 10, 11, 12, 13, 14, 15, 16, 17, 18, 19, 20, 21, 22]). Very often the velocity field is induced by a finite set of forces or generated from a well-known reference mixer that can be controlled in time. This reflects the practical constraint that controlling flow fields

*Department of Mathematics, University of Georgia, Athens, GA 30602, USA (Weiwei.Hu@uga.edu)

†Department of Mathematics, University of Georgia, Athens, GA 30602, USA (mjlai@uga.edu)

‡Department of Mathematics, University of Georgia, Athens, GA 30602, USA (hnwu@uga.edu)

arbitrarily in space is infeasible in real applications (e.g., [5, 23, 9, 24, 25, 14, 26, 18, 27, 28, 29, 30]). Specific strategies include optimizing switching between prescribed flows (e.g. [8, 18, 27]), tuning parameters of ansatz vector fields [26, 31, 32], and refining protocols for prescribed mixers [33, 25, 14], etc. Further research incorporates controlled flow dynamics into the transport and mixing processes can be found in [34, 12, 35, 36, 37, 38, 39, 40, 41, 42].

Our current work introduces a new idea for control of fluid mixing, inspired by the LAP for incompressible flows. Specifically, we aim to find an optimal flow map induced by cellular flows that achieves a desired mixing efficiency with minimal kinetic energy.

1.1 Motivation from LAP for incompressible flows

The classic LAP seeks a smooth curve connecting two given points within the group of volume- and orientation-preserving diffeomorphisms of a compact domain of a Euclidean space, while minimizing the kinetic action. Geometrically, this corresponds to finding a minimal geodesic path in this group as well addressed in the pioneering work of Arnold [43]. The Euler–Lagrange equation associated with its variational formulation yields the Euler equations of incompressible flows in Lagrangian form (e.g. [43]). This problem is formally analogous to the Benamou–Brenier formulation of optimal transport [44], which expresses the Wasserstein (Monge–Kantorovich) distance with quadratic cost as the minimization of kinetic action without an incompressibility constraint.

However, when incompressibility and impermeability conditions are imposed, the resulting optimal flow is governed by Euler equations with two-point boundary values in time, which is notoriously difficult to solve. In fact, even the existence of solutions to this LAP is non-trivial, which necessitates the framework of generalized flows introduced in [2]. Our approach is built up the LAP for incompressible flows, and yet introduces a relaxed criterion that leverages the unique features of mixing processes. In fluid mixing, the essential objective is the degree of mixedness, a quantity not uniquely determined by any single distribution, since different configurations can exhibit the same level of mixedness.

To focus on our discussion, we consider an inhomogeneous passive scalar advected by an incompressible velocity field governed by the transport equation in an open, bounded, and connected domain $\Omega \subset \mathbb{R}^2$. Assume that the boundary of the domain, denoted by Γ , is sufficiently regular (which may include corners). Our objective is to find a velocity field generated by cellular flows that minimizes the kinetic energy while ensuring that the initial scalar distribution reaches a prescribed degree of mixedness by a finite time $t_f > 0$. The resulting optimal control problem is formulated as follows:

$$\min_v \frac{1}{2} \int_0^{t_f} \int_{\Omega} \theta(x, t) |v(x, t)|^2 dx dt, \quad (1.1)$$

$$\text{subject to } \partial_t \theta + v \cdot \nabla \theta = 0, \quad (1.2)$$

$$\nabla \cdot v = 0 \quad \text{with} \quad v \cdot n|_{\Gamma} = 0, \quad (1.3)$$

$$\theta(0) = \theta_0, \quad \text{and} \quad (1.4)$$

$$\|\theta(t_f)\|_m \leq r \|\theta_0\|_m, \quad (1.5)$$

for some given parameter $0 < r < 1$, where n is the unit outer normal vector to the domain boundary Γ and $\|\cdot\|_m$ stands for the mix-norm for quantifying mixing. More details on the mix-norm will be discussed in Section 1.2.

This formulation reframes the search for an optimal transport map from the initial state θ_0 to some final state $\theta(t_f)$ which satisfies a set constraint, as the problem of finding a time-dependent velocity field v that advects θ_0 to some $\theta(t_f)$ under the governing system (1.2)–(1.5), while minimizing the total kinetic energy. Achieving the mixing efficiency is a more natural goal than reaching a precise state. This is exerted by requiring that the mix-norm at final time is reduced to a specified fraction of its initial value. Our formulation essentially leads to a “point to set” type of optimization problem. This draws an essential difference from the classic LAP framework. Moreover, we shall employ cellular flows introduced in Section 1.3 as mixing protocols to construct flow transport maps. This choice not only aligns with physically realizable control mechanisms but also circumvents the analytical challenges associated with infinite-dimensional control problems.

We note that a recent work [45] also develops a fluid mixing framework using dynamic optimal transport but with a prescribed final state. In contrast, our formulation and mixing criteria differ substantially from this setting.

1.2 Mix-norm

A fundamental question in fluid mixing is how to quantify the degree of mixedness. A classical measure is the variance of the scalar concentration, which is equivalent to the L^2 -norm of the scalar field [46]. However, this measure is inadequate in the absence of diffusivity, as it fails to quantify the effects of pure stirring (e.g. [47, 20]). In fact, due to incompressibility and no-penetration boundary condition in (1.3) it can be easily verified that any L^p -norm of θ is conserved, i.e.,

$$\|\theta(t)\|_{L^p(\Omega)} = \|\theta_0\|_{L^p(\Omega)}, \quad t \geq 0, \quad p \in [1, \infty]. \quad (1.6)$$

Mathew, Mezić, and Petzold in [47] first introduced the mix-norm based on ergodic theory, which is sensitive to both stirring and diffusion. They also showed the equivalence of the mix-norm to the $H^{-1/2}$ -norm for periodic boundary conditions. In fact, any negative Sobolev norm H^{-s} , for $s > 0$, that quantifies the weak convergence can be used as a mix-norm (e.g. [15, 17]). Other measures such as the geometric mixing scale, the measure of the interface of the mixtures, as well as entropy are employed to quantify mixing process and the related control problems (e.g. [48, 49, 50, 24, 51, 21, 22, 52]). A more detailed review can be found in [20].

In this work, we consider a general open bounded and connected domain for the scalar field with no additional boundary conditions, where no-penetration is imposed on the velocity field. The dual norm $\|\cdot\|_{(H^s(\Omega))'}$, $s > 0$, is employed to quantify mixing instead of the negative Sobolev norm, where $(H^s(\Omega))'$ is the dual space of $H^s(\Omega)$. Without loss of generality, we adopt $(H^1(\Omega))'$, to quantify mixing following our earlier [36, 39, 37, 40].

To better interpret the dual norm, we consider the elliptic boundary value problem:

$$(-\Delta + I)\eta = \theta \quad \text{in } \Omega, \quad \frac{\partial \eta}{\partial n} \Big|_{\Gamma} = 0. \quad (1.7)$$

The mix-norm is then defined as

$$\|\theta\|_{(H^1(\Omega))'} = \|\eta\|_{H^1(\Omega)}.$$

Let $\mathcal{A} = -\Delta + I$ with domain $D(\mathcal{A}) = \{H^2(\Omega) : \frac{\partial \eta}{\partial n} \Big|_{\Gamma} = 0\}$. Then

$$\|\theta\|_{(H^1(\Omega))'}^2 = (\mathcal{A}^{-1}\theta, \theta). \quad (1.8)$$

Further let $\bar{\theta}_0 := \frac{1}{|\Omega|} \int_{\Omega} \theta_0(x) dx$ denote the spatial average of the initial scalar field. Since the spatial average is conserved for all time, i.e.,

$$\frac{1}{|\Omega|} \int_{\Omega} \theta(x, t) dx = \bar{\theta}_0, \quad \forall t > 0,$$

without loss of generality, we can replace the final time condition (1.5) as

$$\|\theta(t_f) - \bar{\theta}_0\|_{(H^1(\Omega))'}^2 \leq r^2 \|\theta_0 - \bar{\theta}_0\|_{(H^1(\Omega))'}^2, \quad 0 < r < 1. \quad (1.9)$$

1.3 Cellular flows based finite dimensional control design

In this work, we employ cellular flows as two-dimensional mixing protocols, which play a fundamental role in mathematical analysis of fluid mixing and engineering applications (e.g. [53, 54, 50, 10, 51, 55, 13, 56, 57, 58, 18, 59, 52]). Specifically, consider that the flow velocity in (1.2) is induced by a set of finite basis flows in a two-dimensional open unit square $\Omega = (0, 1)^2$:

$$v(x, t) = \sum_{i=1}^N u_i(t) b_i(x), \quad (1.10)$$

where $b_i(x)$, $i = 1, 2, \dots, N$, are the cellular flows generated by the Hamiltonians $H_i(x_1, x_2) = \frac{1}{i\pi} \sin(i\pi x_1) \sin(i\pi x_2)$

$$b_i = \nabla^{\perp} H_i(x_1, x_2) = \begin{bmatrix} -\sin(i\pi x_1) \cos(i\pi x_2) \\ \cos(i\pi x_1) \sin(i\pi x_2) \end{bmatrix}, \quad (1.11)$$

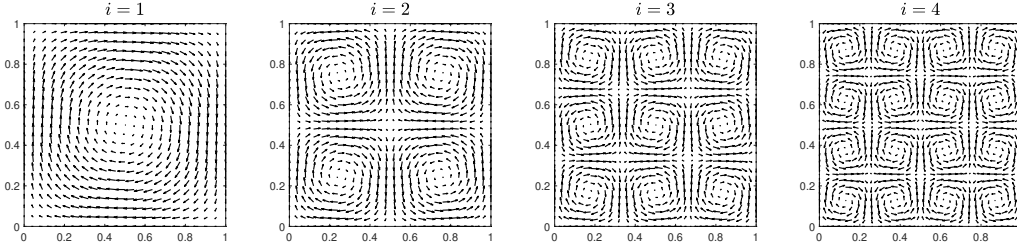


Figure 1: Cellular flows on the square

and the temporal coefficients $u_i(t), i = 1, 2, \dots, N$, serve as the control inputs. It is clear that

$$\nabla \cdot b_i = 0 \quad \text{and} \quad b_i \cdot n|_{\Gamma} = 0. \quad (1.12)$$

Fig. 1 below displays cellular flows b_i for $i = 1, 2, 3, 4$, which comprise i^2 cells.

Cellular flows generated by Hamiltonians are incompressible, periodic flow patterns in a two-dimensional plane that consist of repeating lattices of swirling, closed-loop trajectories. They are especially valuable in regimes where turbulence is unattainable, such as at low Reynolds numbers, or where precise fluid manipulation is required. These protocols are widely employed across scales, from microfluidic devices to industrial-scale reactors, often implemented through designed system geometries (e.g., ridges, baffles, or electrodes) or time-dependent forcing strategies (e.g., flow reversal or rotating fields) that deterministically produce cellular flow structures. For instance, staggered herringbone mixers use patterned grooves on microchannel walls to induce chaotic advection via asymmetric, staggered cellular flows, making them essential for efficient reagent blending in lab-on-a-chip diagnostics. On a larger scale, stirred tank reactors employ rotating impellers to generate intense trailing vortices (small-scale cellular flows) that homogenize contents in chemical and biochemical processes. A central aim of these designs is to transition from orderly cellular flows into chaotic advection, achieving exponential stretching of material lines and ultimately enabling highly efficient mixing.

Mathematically, the velocity field generated by cellular flows preserves the convexity advantages of the Benamou–Brenier framework. As a result, any solution to the problem defined by (1.1)–(1.4) and (1.9) is globally optimal. However, proving the existence of such a solution is nontrivial, as it requires establishing the feasibility of the constraint set—a challenging task within a finite-dimensional control space.

Recent progresses in mathematical analysis of mixing enhancement by cellular flows (e.g. [60, 54, 10, 51, 58, 52]) lay a theoretical foundation for addressing the feasibility of our problem. The details will be discussed in Section 2.

1.4 Organization

The following sections detail the analysis and implementation of our control design. In the next section, we first establish the feasibility of the problem by showing that the constraint set defined by (1.2)–(1.4) and (1.9) together with (1.10)–(1.11) is non-empty for N large enough. We then show in Section 3 that our formulation results in a convex optimization problem and presents the corresponding optimality conditions. The numerical implementation of our control design, including a solution algorithm, is discussed in Section 4. Finally, Section 5 validates our approach with numerical results on a unit square.

In the sequel, the symbol C denotes a generic positive constant, which is allowed to depend on the domain as well as on indicated parameters.

2 Feasibility of the problem

The feasibility of steering the system to a desired degree of mixedness at given final time is closely tied to the bilinear controllability of the system. It becomes particularly challenging when the velocity field is restricted to a finite-dimensional basis. This issue was also noted in work [18] by Matthew *et al.*, where an alternative optimization formulation was pursued. However, our “point to set” type of optimization problem presents a relaxed requirement compared to the demand of controllability.

To start with, we show that for any given initial datum θ_0 , there exists a velocity field spanned by a set of finite dimensional cellular flows such that the final time constraint holds. Our proof will primarily utilize a recent work by Bruè, Coti Zelati, and Marconi in [60], which provides a direct estimate on the mixing rate of the cellular flow and how it is related to the period of the closed orbit generated by its Hamiltonian. In particular, a detailed analysis using action-angle coordinates near the elliptic and hyperbolic points of the Hamiltonian was conducted, as these regions govern the slower mixing rates, to derive an upper bound for the global mixing rate. From this, we further identify the relation between the upper bound and the frequency N of the cellular flows for enhancing mixing. It can be shown that if N is chosen sufficiently large, then the desired mixing level can be achieved by the final time $t_f > 0$ using a single basis flow b_N , and therefore the feasibility of the constraint set follows. We begin by recalling the definition from [60] with a slight modification for general bounded domains.

Definition 2.1 *Let $\gamma: [0, \infty) \rightarrow [0, \infty)$ be a continuous and decreasing function vanishing at infinity. The time-independent velocity field b satisfying (1.3) is mixing with rate $\gamma(t)$ if for every $\theta_0 \in H^1(\Omega)$ with $\theta_0 \notin \ker(b \cdot \nabla)$ we have the following estimate*

$$\|\theta(t_f) - \bar{\theta}\|_{(H^1(\Omega))'} \leq \gamma(t) \|\theta_0 - \bar{\theta}\|_{H^1(\Omega)}, \quad (2.1)$$

for every $t \geq 0$.

Theorem 3 in [60] is key to establishing the feasibility of our problem (1.1)–(1.4) and (1.9). A natural extension of its proof further reveals that increasing the frequency of the cellular flows enhances the mixing rate, as stated below.

Proposition 2.1 *Given any positive integer $N \in \mathbb{Z}^+$, consider the cellular flow $b_N(x_1, x_2) = \nabla^\perp H_N$ in domain $\Omega = (0, 1)^2$:*

1. *if $H_N = \sin(N\pi x_1) \sin(N\pi x_2)$, then for every $\epsilon > 0$ the flow generated by b_N is mixing with rate $\gamma_N(t)$ satisfying*

$$\gamma_N(t) \leq \frac{C_1(\epsilon)}{(N^2 t)^{\frac{1}{3}-\epsilon}}; \quad (2.2)$$

2. *if $H_N = \frac{1}{N\pi} \sin(N\pi x_1) \sin(N\pi x_2)$, then for every $\epsilon > 0$ the flow generated by b_N is mixing with rate $\gamma_N(t)$ satisfying*

$$\gamma_N(t) \leq \frac{C_2(\epsilon)}{(N^{\frac{3}{2}} t)^{\frac{1}{3}-\epsilon}}, \quad (2.3)$$

where $C_1(\epsilon) > 0$ and $C_2(\epsilon) > 0$ in (2.2) and (2.3), respectively, are constants depending on ϵ and the initial condition θ_0 .

We extend the proof established in [60, Theorem 3] for $N = 1$ to an arbitrary frequency N and show how the upper bound of $\gamma_N(t)$ can be lowered by increasing N . The detailed proofs of (2.2)–(2.3) are provided in Appendix A.

To have a uniformly bounded flow basis in time, we employ the estimate (2.3) for the scaled Hamiltonian. For given $t_f > 0$, set

$$\frac{C_2(\epsilon)}{(N^{\frac{3}{2}} t_f)^{\frac{1}{3}-\epsilon}} \leq r \frac{\|\theta_0 - \bar{\theta}\|_{(H^1(\Omega))'}}{\|\theta_0 - \bar{\theta}\|_{H^1(\Omega)}}.$$

If N is chosen to satisfy

$$N \geq \left\lceil \left[\left(\frac{C_2(\epsilon) \|\theta_0 - \bar{\theta}\|_{H^1(\Omega)}}{r \|\theta_0 - \bar{\theta}\|_{(H^1(\Omega))'}} \right)^{\frac{2}{1-3\epsilon}} \frac{1}{t_f^{\frac{2}{3}}} \right] \right\rceil, \quad (2.4)$$

where $\lceil \cdot \rceil$ stands for the ceiling function, then the constraint set defined by (1.2)–(1.4) and (1.9) is nonempty, and hence our minimization problem (1.1) is feasible.

Although a single high-frequency cellular flow can achieve the desired mixing level by the final time, its efficiency is limited by the underlying dynamics. In such a flow, fluid particles follow the contour lines of the Hamiltonian $H_N(x_1, x_2)$ forming a grid of vortices where particles are confined to closed orbits within individual cells. Consequently, particles cannot transport across the cell boundaries to achieve efficient global mixing. In contrast, a linear combination of flows with different frequencies disrupts this structure, generating trajectories that cross these barriers and alter the elliptic and hyperbolic regions where slow mixing typically occurs.

3 Existence and the first-order optimality conditions

In this section, we first establish the existence of a global solution to (1.1)–(1.4) and (1.9) using the Benamou–Brenier formulation in optimal transport [44], for N satisfying condition (2.4).

For notational convenience, we let

$$\vec{u}(t) = [u_1(t), u_2(t), \dots, u_N(t)]^T$$

and

$$\vec{b}(x) = [b_1(x), b_2(x), \dots, b_N(x)]^T.$$

Here we choose $U_{ad} = (L^2(0, t_f))^N$ as the set of admissible controls. Then according to (1.6), it is easy to verify that the kinetic energy defined in (1.1) is finite for any $\theta_0 \in L^\infty(\Omega)$ and $\vec{u} \in U_{ad}$.

Theorem 3.1 *Let $\theta_0 \in L^\infty(\Omega) \cap H^1(\Omega)$ with $\theta_0 \geq 0$. For $t_f > 0$, $0 < r < 1$, and frequency N satisfying (2.4), the optimal control problem governed by (1.1)–(1.4) and (1.9) is convex and admits a global optimal solution.*

Proof. Let $m(x, t) = \vec{u}(t)^T \vec{b}(x) \theta(x, t)$. From the conditions in (1.12) we have

$$\nabla \cdot \left(\frac{m}{\theta} \right) = 0 \quad \text{and} \quad \frac{m}{\theta} \cdot n|_\Gamma = 0,$$

for any control $\vec{u}(t) \in U_{ad}$. Thus problem (1.1)–(1.4) and (1.9) can be rewritten as

$$\min J(m, \theta) := \frac{1}{2} \int_0^{t_f} \int_\Omega \frac{|m(x, t)|^2}{\theta(x, t)} dx dt \quad (3.1)$$

$$\text{subject to } \frac{\partial \theta}{\partial t} + \nabla \cdot m = 0, \quad (3.2)$$

$$\theta(x, 0) = \theta_0(x), \quad (3.3)$$

$$\|\theta(t_f) - \bar{\theta}_0\|_{(H^1(\Omega))'}^2 \leq r^2 \|\theta_0 - \bar{\theta}_0\|_{(H^1(\Omega))'}^2. \quad (3.4)$$

The constraint set defined by (1.2)–(1.4) and (1.9) is nonempty provided N satisfies (2.4). To establish convexity, we show that the problem minimizes a convex functional over a convex constraint set.

Convex functional. For $\theta \geq 0$, the function $|m|^2/\theta$ represents the perspective function (e.g. [61]) of the convex quadrature $l(m) = |m|^2$. As perspective operations preserve convexity, the convexity of the cost functional follows immediately. Note that $|m|^2/\theta = 0$ if $\theta = 0$.

Convex constraint set. The nonempty constraint set defined by (3.2)–(3.4) is convex because constraints (3.2)–(3.3) are linear in m and θ , and the inequality constraint (3.4) is convex. Therefore, problem (3.1)–(3.4) is convex and admits a global solution, as does the equivalent problem (1.1)–(1.4) and (1.9). \square

Remark 3.1 *Although the optimal control problem (3.1)–(3.4) is convex, its strong convexity is not guaranteed, and thus a unique global minimizer is not guaranteed.*

To derive the first-order necessary conditions of optimality for the optimal control problem, we employ an Euler-Lagrange approach. These conditions are also sufficient for a global minimum due to convexity. The differentiability of the Lagrangian is justified by the following regularity of the problem: since \vec{b} is sufficiently smooth, for $\theta_0 \in L^\infty(\Omega) \cap H^1(\Omega)$ and $\vec{u} \in (L^2(0, t_f))^N$, the solution to the transport equation satisfies $\theta \in L^\infty(0, t_f; L^\infty(\Omega) \cap H^1(\Omega))$ (e.g. [36, 37]). This regularity ensures the Gâteaux differentiability of the control-to-state map $\vec{u} \mapsto \theta$ and, consequently, of the cost functional J . A global optimal solution to problem (1.1)–(1.4) and (1.9) is therefore characterized by the following conditions.

Theorem 3.2 Let $\theta_0 \in L^\infty(\Omega) \cap H^1(\Omega)$ with $\theta_0 \geq 0$. For $t_f > 0$, $0 < r < 1$, and frequency N satisfying (2.4), (\vec{u}, θ) is an optimal solution to the problem governed by (1.1)–(1.4) and (1.9) if and only if there exist $\rho \in L^\infty(0, t_f; L^\infty(\Omega)) \cap H^1(\Omega)$ and $\lambda \geq 0$ such that

1. **State Equation:**

$$\partial_t \theta + \sum_{i=1}^N u_i (b_i \cdot \nabla \theta) = 0, \quad \theta(x, 0) = \theta_0(x), \quad (3.5)$$

with the final-time constraint:

$$\|\theta(t_f) - \bar{\theta}_0\|_{(H^1(\Omega))'}^2 \leq r^2 C_0^2; \quad (3.6)$$

where $C_0 := \|\theta_0 - \bar{\theta}_0\|_{(H^1(\Omega))'}$;

2. **Adjoint Equation:**

$$\begin{aligned} -\partial_t \rho - \sum_{i=1}^N u_i (b_i \cdot \nabla \rho) &= \frac{1}{2} \sum_{i=1}^N |u_i b_i|^2, \\ \rho(t_f) &= -2\lambda \mathcal{A}^{-1} \theta(t_f), \end{aligned} \quad (3.7)$$

where $\mathcal{A}^{-1} \theta(t_f)$ satisfies the elliptic problem (1.7);

3. **Optimality Condition:**

$$\vec{u}(t) = \mathbf{M}^{-1}(t) \mathbf{p}(t), \quad (3.8)$$

where $\mathbf{M}(t) \in \mathbb{R}^{N \times N}$ is a matrix with entries $M_{ij}(t) := \int_{\Omega} \theta b_i \cdot b_j \, dx$ and $\mathbf{p}(t) \in \mathbb{R}^N$ is a vector with entries $p_i(t) := \int_{\Omega} (b_i \cdot \nabla \rho) \theta \, dx$;

4. **Complementary Slackness:**

$$\lambda \left(\|\theta(t_f) - \bar{\theta}_0\|_{(H^1(\Omega))'}^2 - r^2 C_0^2 \right) = 0, \quad \lambda \geq 0. \quad (3.9)$$

Proof. First we introduce the Lagrangian

$$\begin{aligned} &\mathcal{L}(\theta, \vec{u}, \theta(t_f); \rho, \lambda) \\ &= J(\theta, \vec{u}) - \underbrace{\left[\int_0^{t_f} \int_{\Omega} \rho \left(\partial_t \theta + \sum_{i=1}^N u_i (b_i \cdot \nabla \theta) \right) \, dx \, dt \right]}_{\text{PDE constraint}} \\ &\quad + \underbrace{\lambda \left(\|\theta(t_f) - \bar{\theta}_0\|_{(H^1(\Omega))'}^2 - r^2 C_0^2 \right)}_{\text{Terminal constraint}}, \end{aligned} \quad (3.10)$$

where ρ is the Lagrange multiplier or the adjoint state corresponding to θ and $\lambda \geq 0$ is the KKT multiplier. By Stokes formula and conditions given by (1.12) we have

$$\begin{aligned} &\int_{\Omega} \rho \left(\sum_{i=1}^N u_i (b_i \cdot \nabla \theta) \right) \, dx = \sum_{i=1}^N u_i \int_{\Omega} \rho \nabla \cdot (b_i \theta) \, dx \\ &= \sum_{i=1}^N u_i \left(\int_{\Gamma} \rho (b_i \theta) \cdot n \, dx - \int_{\Omega} \nabla \rho \cdot (b_i \theta) \, dx \right) \\ &= - \sum_{i=1}^N u_i \int_{\Omega} (b_i \cdot \nabla \rho) \theta \, dx. \end{aligned} \quad (3.11)$$

Applying integration by parts to the second term on the right hand side of (3.10) together with (3.11) and (1.8) follows

$$\begin{aligned}
& \mathcal{L}(\theta, \bar{u}, \theta(t_f); \rho, \lambda) \\
&= \frac{1}{2} \int_0^{t_f} \int_{\Omega} \theta \left| \sum_{i=1}^N u_i b_i \right|^2 dx dt - \left[(\rho(t_f), \theta(t_f)) - (\rho_0, \theta_0) \right. \\
& \quad \left. + \int_0^{t_f} \int_{\Omega} (-\partial_t \rho \theta) dx dt - \sum_{i=1}^N \int_0^{t_f} u_i \left(\int_{\Omega} (b_i \cdot \nabla \rho) \theta dx \right) dt \right. \\
& \quad \left. + \lambda \left((\mathcal{A}^{-1} \theta(t_f) - \bar{\theta}_0, \theta(t_f) - \bar{\theta}_0) - r^2 C_0^2 \right) \right],
\end{aligned}$$

where in last term we used $\mathcal{A}^{-1} \bar{\theta}_0 = \bar{\theta}_0$. The adjoint state ρ is chosen such that the first derivatives of \mathcal{L} with respect to θ vanishes, i.e. $\frac{\partial \mathcal{L}}{\partial \theta} = 0$, which results in (3.7). The final-time condition (3.7) is derived by setting $\frac{\partial \mathcal{L}}{\partial \theta(t_f)} = 0$. Now setting $\frac{\partial \mathcal{L}}{\partial u_i} = 0$ for each $i = 1, 2, \dots, N$, follows

$$\sum_{j=1}^N u_j \left(\int_{\Omega} \theta b_j \cdot b_j dx \right) - \int_{\Omega} (b_j \cdot \nabla \rho) \theta dx = 0.$$

Let $\mathbf{M}(t) \in \mathbb{R}^{N \times N}$ be a matrix with entries $M_{ij}(t) := \int_{\Omega} \theta b_i \cdot b_j dx$ and $\mathbf{p}(t) \in \mathbb{R}^N$ is a vector with entries $p_i(t) := \int_{\Omega} (b_i \cdot \nabla \rho) \theta dx$. Then the optimality condition for \bar{u} becomes (3.8). Lastly, we require that the KKT multiplier λ for the final-time constraint satisfies the complimentary slackness condition, that is,

$$\lambda \left(\|\theta(t_f) - \bar{\theta}_0\|_{(H^1(\Omega))'}^2 - r^2 C_0^2 \right) = 0. \quad (3.12)$$

If the optimal KKT multiplier $\lambda > 0$, then the constraint (1.9) is active, meaning the inequality is satisfied as an equality at the optimum. The detailed explanation on a Lagrangian-based view of the adjoint approach can be found in [62, p. 63, 1.6.4]. \square

4 Numerical implementation

The optimality conditions derived in Theorem 3.2 can be solved via the fixed-point iteration

$$\begin{bmatrix} u^{k+1} \\ \lambda^{k+1} \end{bmatrix} = \begin{bmatrix} F_1(u^k, \lambda^k) \\ F_2(u^k, \lambda^k) \end{bmatrix},$$

where the mapping F_1 encodes the coupled system given by the state equation (3.5), the adjoint equation (3.7), and the optimality condition (3.8), and the mapping F_2 incorporates both the final time condition (3.6) and the complementary slackness condition (3.9). Specifically, conditions (3.6) and (3.9) can be solved using the following fixed-point iteration

$$\lambda^{k+1} = \max \left(\lambda^k + \beta^k \left(\|\theta^k(t_f) - \bar{\theta}_0\|_{(H^1(\Omega))'}^2 - r^2 C_0^2 \right), 0 \right), \quad (4.1)$$

where $\beta^k > 0$ is a step-size parameter. At convergence, we recover

$$\lambda^* = \max \left(\lambda^* + \beta^* \left(\|\theta^*(t_f) - \bar{\theta}_0\|_{(H^1(\Omega))'}^2 - r^2 C_0^2 \right), 0 \right)$$

for some $\beta^* > 0$, which implies $\lambda^* \geq 0$ and

$$\begin{cases} \text{if } \|\theta^*(t_f) - \bar{\theta}_0\|_{(H^1(\Omega))'}^2 - r^2 C_0^2 < 0, \text{ then } \lambda^* = 0, \\ \text{if } \lambda^* > 0, \text{ then } \|\theta^*(t_f) - \bar{\theta}_0\|_{(H^1(\Omega))'}^2 - r^2 C_0^2 = 0, \end{cases}$$

precisely satisfying conditions (3.6) and (3.9). In particular, when updating u^{k+1} , we introduce a relaxation factor $\alpha^{k+1} \in (0, 1]$ to control the update:

$$u^{k+1} = (1 - \alpha^{k+1})u^k + \alpha^{k+1} \mathbf{M}_{k+1}^{-1} \mathbf{p}_{k+1}, \quad (4.2)$$

where $\mathbf{M}_{k+1} \in \mathbb{R}^{N \times N}$ and $\mathbf{p}_{k+1} \in \mathbb{R}^N$ with entries $\int_{\Omega} \theta^{k+1} b_i \cdot b_j dx$ and $\int_{\Omega} \theta^{k+1} \nabla \rho^{k+1} \cdot b_i dx$, respectively. This relaxation enhances stability by preventing overshooting and oscillations between iterations.

Let

$$\mu^{k+1} = \|\theta^{k+1}(t_f)\|_{(H^1(\Omega))'}^2 - r^2 C_0^2$$

be the final-time constraint violation for iterating θ^{k+1} and set $0 < \varepsilon_1, \varepsilon_2 \ll 1$ as the stopping criteria parameters. We propose the following Algorithm 1 to solve the first-order optimality conditions governed by (3.5)–(3.9). For spatial discretization, we adopt the spline collocation method (e.g. [63, 64]), with bivariate splines serving as the basis functions for approximating numerical solutions in space (e.g. [65, 66]). For the temporal aspect, the implicit Euler scheme is used for the state equation (3.5), while the explicit Euler scheme is applied to the (backward) adjoint equation (3.7).

Algorithm 1: Fixed-point iteration for the optimal control problem (1.1)–(1.4) and (1.9)

Input: u^0 , initial data θ_0 , final time t_f , parameter $\lambda^0 > 0$, stopping criteria $0 < \varepsilon_1, \varepsilon_2 \ll 1$

repeat

 Solve the state equation (3.5) with u^k for θ^{k+1} ;

 Solve the equation (1.7) with θ^{k+1} for η^{k+1} ;

 Update β^{k+1} and update λ^{k+1} via (4.1); Solve the adjoint equation (3.7) with $\theta^{k+1}(t_f)$ for ρ^{k+1} ;

 Update α^{k+1} and update u^{k+1} via (4.2);

until $\mu^{k+1} \leq \varepsilon_1$ and $|J(u^{k+1}) - J(u^k)|/|J(u^k)| \leq \varepsilon_2$;

5 Numerical results

As illustrated in Fig. 1, the streamlines of the cellular flows within each cell form closed circular patterns and are tangent to, but do not cross, those of adjacent cells. This structure prevents particles from accessing the entire domain by trapping them in localized regions. To address this limitation, we explore the use of linear combinations of cellular flows of different frequency. The key idea is that if a particle is trapped in one cell, activating a different flow can transport it across the cell boundaries to achieve more global mixing. In our numerical experiments, we investigate three different combinations: $i = 1$ & 2, $i = 1$ & 3, and $i = 1$ & 4, all simulated up to a final time of $t_f = 1$.

For the numerical solution of PDEs, we employ a spline-based solver with a mesh size (i.e., the length of the longest edge in the triangulation) of $h = 0.0884$ and a time step of $\tau = 0.005$. The optimization algorithm is initialized with $\lambda^0 = 1$, and the convergence criteria are set to $\varepsilon_1 = 5\mathbf{e}-4$ and $\varepsilon_2 = 1\mathbf{e}-3$. Additionally, we implement adaptive update strategies for α^k and β^k :

$$\alpha^{k+1} = \begin{cases} \max(0.5\alpha^k, 0.05) & \text{if } \mu^{k+1} < \varepsilon_1, \\ \alpha^k & \text{otherwise,} \end{cases}$$

and

$$\beta^{k+1} = \begin{cases} \frac{2J(u^k, \theta^{k+1})}{\mu^{k+1}} & \text{if } \mu^{k+1} \geq \varepsilon_1 \text{ and } J(u^k, \theta^{k+1}) \geq 1, \\ 100 & \text{if } \mu^{k+1} \geq \varepsilon_1 \text{ and } J(u^k, \theta^{k+1}) < 1, \\ 250 & \text{if } \mu^{k+1} < \varepsilon_1. \end{cases}$$

For the control parameters, we set $r = 0.3$ in the final time constraint (1.9) and the initial control inputs as $u_1(t) = 0$ and $u_i(t) = 1$, $i = 2, 3, 4$, for $t \in [0, 1]$, for each combination. This initial configuration activates the multi-cell flows while keeping the single-cell flow idle. Two types of initial data are investigated in our numerical experiments. First consider

$$\theta_0(x_1, x_2) = \tanh\left(\frac{2x_2 - 1}{0.2}\right) + 1,$$

which approximates a bicolor distribution, yet satisfies the regularity required in Theorem 3.2. The optimal mixing results under various combinations of cellular flows are displayed in Fig. 2. As time evolves, the scalar field becomes progressively more mixed as finer and finer structures develop. The

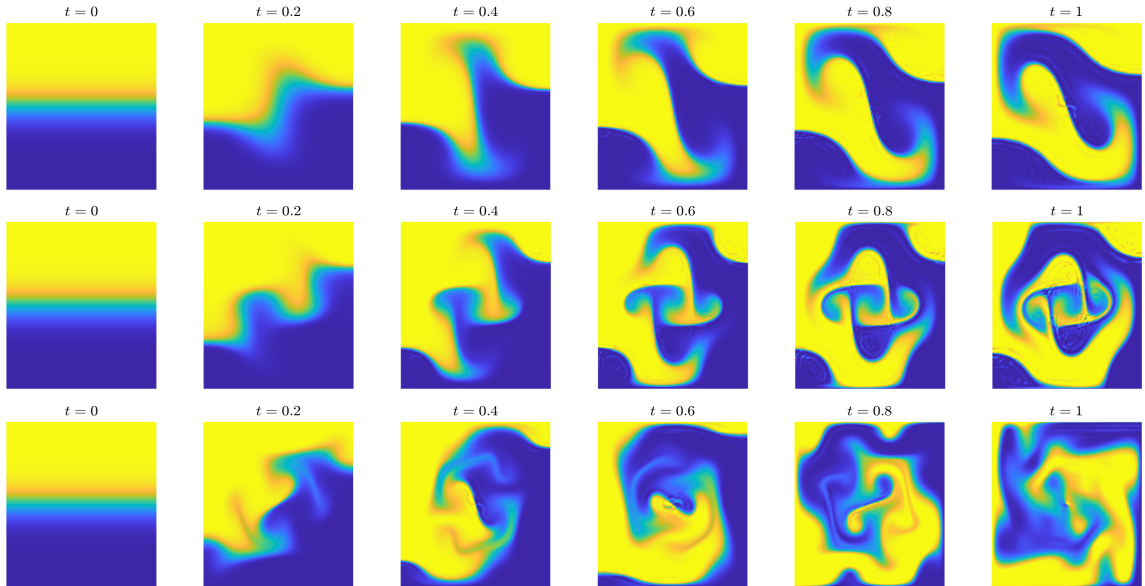


Figure 2: Snapshots of the optimal mixing at $t = 0, 0.2, 0.4, 0.6, 0.8, 1$, for the initial datum $\theta_0(x_1, x_2) = \tanh((2x_2 - 1)/0.2) + 1$ in the unit square – **Top:** b_1 & b_2 ; **Middle:** b_1 & b_3 ; **Bottom:** b_1 & b_4

detailed quantifications of the system performance under each optimal control are shown in Fig. 3. In particular, we compare mixing under constant control inputs as the initial configuration versus our optimal strategy. The former employs only a single flow basis function in each experiment, activated consistently throughout the entire simulation.

The first column of Fig. 3 compares the mix-norms for the constant input case (dashed line), the optimal input case (red solid line), and the target level rC_0 . The mix-norm for the constant case shows little decay, whereas the optimal case converges to the target, demonstrating a substantial improvement. As shown in the last two columns of Fig. 3, the optimal protocol activates both the single-cell flow $u_1(t)$ and multi-cell flows $u_i(t), i = 2, 3, 4$, achieving effective mixing through their combination. It is worth noting that a sign change in the controls indicates a required reversal of flow orientation, as shown in the last plot of the fourth column.

The optimality of our control design is supported by two results in Fig. 3. First, the relative error of the cost functional converges, as shown in the second column. Second, the complementary slackness condition (see Eq. (3.9) in Theorem 3.2) is satisfied. Our computed optimal KKT multiplier is non-zero, indicating an active final-time constraint. This is visually confirmed by the mixing result with the optimal control (red solid line) reaching and tracking the target (dotted line) in the first column.

We next examine a second initial distribution given by

$$\theta_0(x_1, x_2) = \sin(2\pi x_2) + 1,$$

using the same configuration as in the first case. This yields analogous numerical results, with the mixing outcomes and optimal control profiles displayed in Figs. 4 and 5.

Our analysis and numerical implementation can be extended to other domains, provided that cellular flows are suitably defined and satisfy the non-penetration boundary condition in (1.12).

6 Conclusion

This paper proposes a control design of fluid mixing problem, drawing inspiration from the LAP for incompressible flows. A fundamental departure from the classic framework is the specification of a *constraint set* of acceptable final states in terms of mix-norms, rather than a single target. This is more natural setup for mixing applications, as it emphasizes a desired degree of mixedness without requiring an exact final configuration. We represent our control velocity in terms of two-dimensional cellular flows, whose structure inherently satisfies incompressibility and no-penetration boundary conditions.

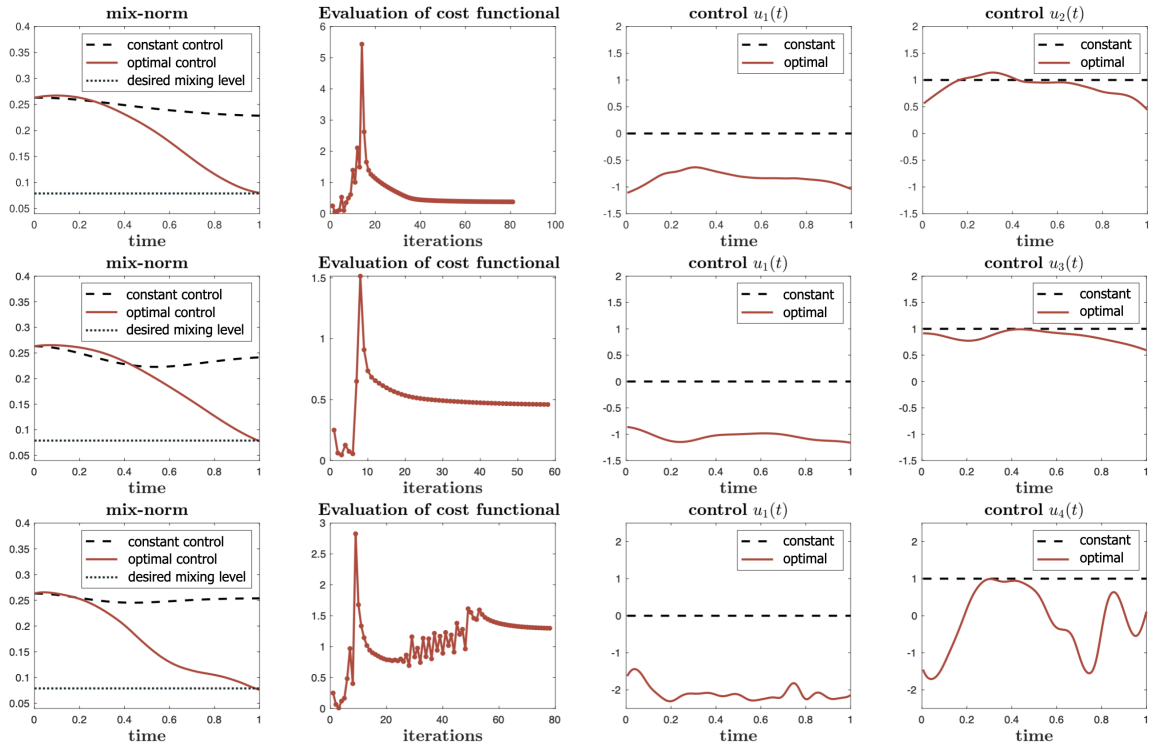


Figure 3: Quantification of system performance in the unit square – **Top:** b_1 & b_2 ; **Middle:** $i = b_1$ & b_3 ; **Bottom:** $i = b_1$ & b_4

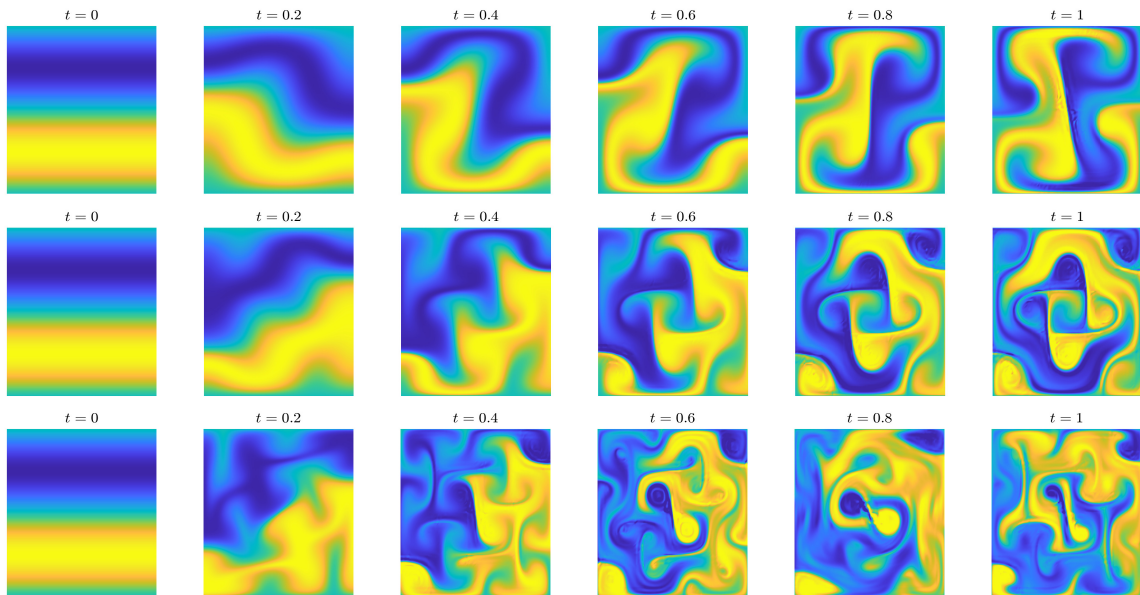


Figure 4: Snapshots of the optimal mixing at $t = 0, 0.2, 0.4, 0.6, 0.8, 1$, for the initial datum $\theta_0(x_1, x_2) = \sin(2\pi x_2) + 1$ in the square – **Top:** b_1 & b_2 ; **Middle:** $i = b_1$ & b_3 ; **Bottom:** $i = b_1$ & b_4

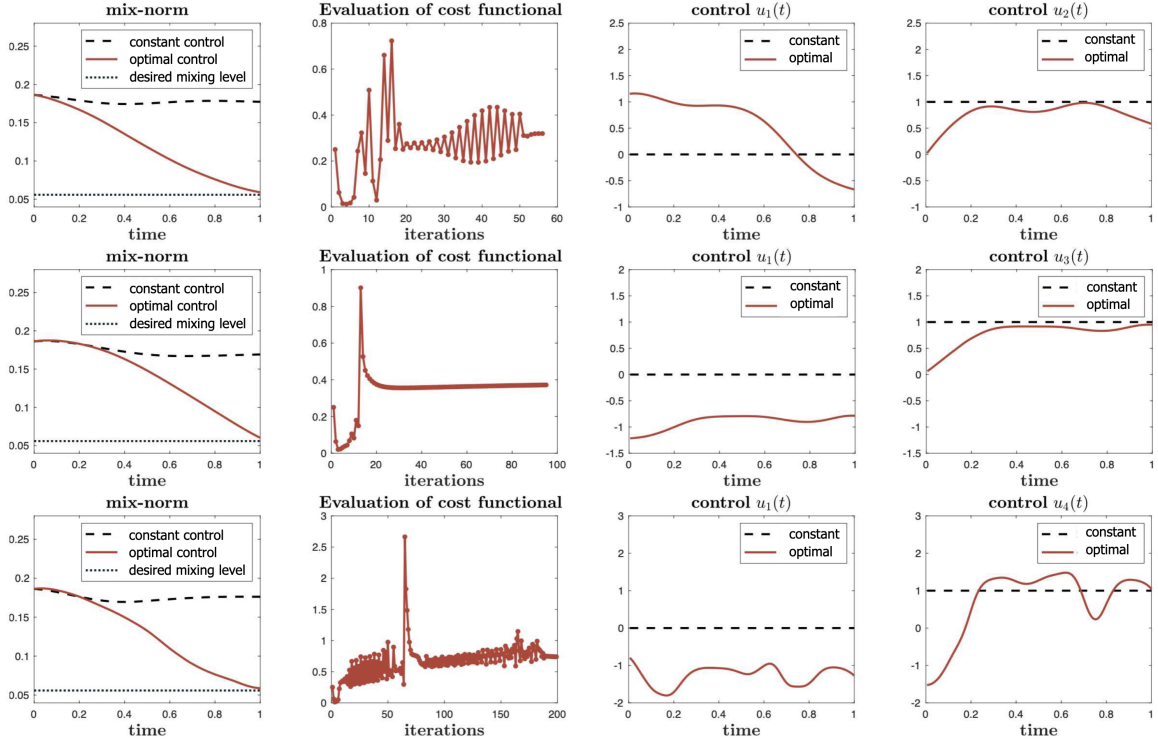


Figure 5: Quantification of system performance in the square – **Top:** b_1 & b_2 ; **Middle:** $i = b_1$ & b_3 ; **Bottom:** $i = b_1$ & b_4

A critical theoretical challenge is whether the imposed constraint set is feasible under cellular flow mixing protocols. To address this, we generalize a recent result by [60] on the mixing rate of the cellular flow, establishing that the mixing rate can be enhanced by increasing the flow frequency. Then we show that our control design preserves the convexity advantages of the Benamou–Brenier formulation. The resulting optimal control problem (1.1)–(1.4) and (1.9) is convex and admits global optimal solutions. Finally, we derive the optimality conditions for the control problem and propose a fixed-point iteration to compute the optimal control. Numerical simulations demonstrate that our design successfully produces controls that satisfy the specified mix-norm constraint.

The constructive approximation of our control design using divergence-free basis flows is critical, as it preserves the convexity inherent in the Benamou–Brenier optimal transport formulation. For a general divergence-free velocity field, convexity is not guaranteed because the corresponding condition $\nabla \cdot (m/\theta)$, which is automatically satisfied with cellular-flow mixing protocols, breaks the convex structure. This approximation framework can also be extended to other divergence-free bases, provided the feasibility of achieving the desired mix-norm with these flows is established.

Our numerical experiments confirm that linear combinations of different cellular flows achieve more efficient mixing by facilitating transport across cell boundaries, thereby inducing more chaotic advection. However, a qualitative description of the mixing rate for such combinations remains open. The investigation of this description, along with other possible Hamiltonian flow protocols for effective mixing, is one of the central directions for our future work.

Appendix A: Sketch of the proof of Proposition 2.1

Proposition 2.1 is a direct extension of the result by Bruè, Coti Zelati, and Marconi [60, Theorem 3] for the cellular flow generated by the Hamiltonian $H_c = \sin(x_1)\sin(x_2)$ in a two-dimensional torus \mathbb{T}^2 . This work estimates the mixing rate by linking it to the period of the closed Hamiltonian orbit. In particular, it hinges on a detailed analysis using action-angle coordinates for mixing near elliptic and hyperbolic points, which is necessary to account for the slower mixing in these regions.

Lemma A1([60, Theorem 3]) *Consider the standard cellular flow $b_c = \nabla^\perp H_c$ with $H_c(x_1, x_2) = \sin x_1 \sin x_2$ on \mathbb{T}^2 , a two-dimensional torus. Then for every $\epsilon > 0$ the vector field b_c is mixing with*

rate

$$Ct^{-1} \leq \gamma_c(t) \leq C(\epsilon)t^{-\frac{1}{3}+\epsilon} \quad (6.1)$$

The inequalities hold up to a universal constant C and a constant $C(\epsilon)$ depending on ϵ , respectively. Here $\epsilon > 0$ is an arbitrarily small constant. Since the Hamiltonian H_c is 2π -periodic and the flow field is symmetric with respect to the lines $x_1 = \pi$ and $x_2 = \pi$, the analysis in [60] was sufficiently performed over the domain $[0, \pi]^2$. The cellular flow also naturally satisfies the no-penetration boundary condition on the boundary of each cell. These properties allow us to generalize the proof to the bounded domain $\Omega = (0, 1)^2$ using Hamiltonians $H_i(x_1, x_2) = \sin(i\pi x_1) \sin(i\pi x_2)$ or the scaled one $H_i(x_1, x_2) = \frac{1}{i\pi} \sin(i\pi x_1) \sin(i\pi x_2)$, for $i = 1, 2, \dots, N$.

In the following discussion, we present the necessary tools and results from [60] to prove (6.1) for the cellular flows generated by the Hamiltonians H_N with an arbitrary positive frequency N and show that the upper bound coefficient $C(\epsilon)$ can be lowered by increasing N .

A1. Action-Angle Coordinates

The action-angle coordinates will be used to facilitate the estimation of the mix-norm. For the convenience of numerical implementation, we set $\Omega = (0, 1)^2$. Note that the Hamiltonian H_N has period $\frac{2}{N}$ in both x_1 and x_2 , resulting in N^2 identical cells tiling Ω . Since the dynamics of the scalar field is confined to each cell, it suffices to restrict our discussion to the fundamental cell $[0, \frac{1}{N}] \times [0, \frac{1}{N}]$.

Consider the transport equations (1.2)–(1.3) with $\theta(0) = \theta_0$ and its associated flow $X: \mathbb{R} \rightarrow \Omega$ defined as the solution to the ODE

$$\partial_t X(t, x) = v(t, X(t, x)), \quad X(0, x) = x. \quad (6.2)$$

Let $(h_0, h_1) \subset H_N(\Omega)$ and $\Omega_0 := H_N^{-1}((h_0, h_1)) \subset (0, \frac{1}{N})$. Given $h \in (h_0, h_1)$, we let $T_N(h)$ be the period of the closed orbit $\{H_N = h\}$. Then $x = x(h): (h_0, h_1) \rightarrow \Omega_0$ solves the following ODE

$$x'(h) = \frac{\nabla H_N}{|\nabla H_N|^2}(x(h)), \quad x(h_0) = x_0. \quad (6.3)$$

Based on the flow map in (6.2), one can define the coordinates $\Phi_N: S^1 \times (h_0, h_1) \rightarrow \Omega_0$ by

$$\Phi_N(\vartheta, h) := X(\vartheta T_N(h), x(h)), \quad (6.4)$$

where $S^1 = [0, 1)$. Note that (see, e.g. [60, (2.7)])

$$|\det D\Phi_N(\vartheta, h)| = T_N(h). \quad (6.5)$$

A2. Hamiltonian $H_N = \sin(N\pi x_1) \sin(N\pi x_2)$

For Hamiltonian $H_N = \sin(N\pi x_1) \sin(N\pi x_2)$ with $N \in \mathbb{Z}^+$, we further consider the coordinates

$$\begin{aligned} \tilde{\Phi}_N: S^1 \times \left(0, \frac{1}{2N}\right) &\rightarrow \left(0, \frac{1}{N}\right)^2 \setminus \left\{\left(\frac{1}{2N}, \frac{1}{2N}\right)\right\}, \\ \tilde{\Phi}_N(\vartheta, I) &= X\left(\vartheta \tilde{T}_N(I), \left(\frac{1}{2N}, I\right)\right), \end{aligned} \quad (6.6)$$

where $\tilde{T}_N(I)$ is the period of the closed orbit in $\{H_N = \sin(N\pi I)\}$ passing through the point $(1/2N, I)$. These coordinates are related to the action-angle coordinates (6.4) by

$$\begin{aligned} \tilde{\Phi}_N(\vartheta, I) &= \Phi(\vartheta, \sin(N\pi I)), \\ \tilde{T}_N(I) &= T_N(\sin(N\pi I)) = \frac{4}{N^2\pi^2} K(\cos(N\pi I)), \end{aligned} \quad (6.7)$$

where

$$K(k) = \int_0^{\frac{\pi}{2}} \frac{d\vartheta}{\sqrt{1 - k^2 \sin^2(\vartheta)}}, \quad -1 < k < 1, \quad (6.8)$$

is the complete elliptic integral of the first kind. Then $f(t, \vartheta, I) := \theta(t, \tilde{\Phi}(\vartheta, I))$ solves the equation

$$\partial_t f + \frac{\partial_\vartheta f}{\tilde{T}_N(I)} = 0 \text{ for } (t, \vartheta, I) \in \mathbb{R} \times \mathbb{S}^1 \times \left[0, \frac{1}{2N}\right]. \quad (6.9)$$

With the help of (6.5) and (6.7), we have

$$J_{\tilde{\Phi}_N}(\vartheta, I) = N\pi J_{\Phi_N}(\vartheta, \sin(N\pi I)) \cos(N\pi I) = N\pi \tilde{T}_N(I) \cos(N\pi I). \quad (6.10)$$

Let

$$g_N(I) := N\pi \tilde{T}_N(I) (\cos N\pi I) \quad (6.11)$$

and consider the weighted Sobolev space H_g^1 defined by

$$\|f\|_{H_g^1} := \int_{\mathbb{S}^1 \times (0, \frac{1}{2N})} (|f(\vartheta, s)|^2 + |\partial_s f(\vartheta, s)|^2) g(s) ds d\vartheta.$$

The following result from [60, Lemma A.1] provides a crucial bridge to understand the negative Sobolev space in terms of the action-angle coordinates.

Lemma A2 ([60, Lemma A.1]) *Let $\theta = \theta(t, x)$ and $f(t, \vartheta, s) = \theta(t, \Phi(\vartheta, s))$ for some change of coordinate Φ . Assume that the Jacobian $J_\Phi(\vartheta, s) = g(s)$ for some smooth positive function g . If*

$$\sup_{\|\phi\|_{H_g^1} \leq 1} \int f(t, \vartheta, s) \phi(\vartheta, s) g(s) ds \leq \|f(0, \cdot)\|_{H_g^1} r(t)$$

for some $r(t)$, then

$$\|\theta\|_{H^{-1}} \leq \|\theta_0\|_{H^1} (1 + \text{Lip}(\Phi))^2 r(t),$$

where $\text{Lip}(\Phi)$ is the Lipschitz constant of Φ given by $\text{Lip}(\Phi) = \sup_{(\vartheta, s) \in \Omega} \|D\Phi(\vartheta, s)\|$.

Assume that $\rho_0 \in C^1(\Omega)$ be mean zero along the level sets of H_N . For fixed $\delta_\epsilon, \delta_h \in (0, \frac{1}{2N})$, we have

$$\sup_{\|\phi\|_{H_{g_N}^1} \leq 1} \int_{\delta_h}^{\frac{1}{2N} - \delta_\epsilon} \int_{\mathbb{S}^1} f(t, \vartheta, s) \phi(\vartheta, s) g_N(s) d\vartheta ds \leq \|f(0, \cdot)\|_{H_{g_N}^1} r_N(t),$$

where

$$\begin{aligned} r_N(t) &= \frac{1}{N\pi t} \|g_N^{-\frac{1}{2}}\|_{L^2(\delta_h, \frac{1}{2N} - \delta_\epsilon)}^2 \left(\frac{\tilde{T}_N^2(\delta_h) g_N(\delta_h)}{|\tilde{T}'_N|} + \frac{\tilde{T}_N^2(\frac{1}{2N} - \delta_\epsilon) g_N(\frac{1}{2N} - \delta_\epsilon)}{|\tilde{T}'_N|} \right) \\ &+ \left\| \left(\frac{\tilde{T}_N^2 g_N}{\tilde{T}'_N} \right)' \right\|_{L^1(\delta_h, \frac{1}{2N} - \delta_\epsilon)} + \left\| \frac{\tilde{T}_N^2 g_N^{\frac{1}{2}}}{\tilde{T}'_N} \right\|_{L^2(\delta_h, \frac{1}{2N} - \delta_\epsilon)} \\ &+ \frac{1}{N\pi t} \|g_N^{-\frac{1}{2}}\|_{L^2(\delta_h, \frac{1}{2N} - \delta_\epsilon)} \left\| \frac{\tilde{T}_N^2 g_N^{\frac{1}{2}}}{\tilde{T}'_N} \right\|_{L^2(\delta_h, \frac{1}{2N} - \delta_\epsilon)} \end{aligned} \quad (6.12)$$

is derived in the proof of [60, Theorem 5] and g_N is defined by (6.11).

To estimate $r_N(t)$, we need to estimate $\tilde{T}_N, \tilde{T}'_N$ and \tilde{T}''_N . In light of (6.7), we know that when $I \rightarrow 0$, $K(\cos(N\pi I)) \rightarrow \ln(\frac{4}{N\pi I})$, and hence

$$\tilde{T}_N(I) \sim \frac{4}{N^2 \pi^2} \ln\left(\frac{4}{N\pi I}\right), \quad \text{as } I \rightarrow 0.$$

When $I \rightarrow \frac{1}{2N}$, $K(\cos(N\pi I)) \rightarrow \frac{\pi}{2}$, thus

$$\tilde{T}_N(I) \sim \frac{4}{N^2 \pi^2} \cdot \frac{\pi}{2} = \frac{2}{N^2 \pi}, \quad \text{as } I \rightarrow \frac{1}{2N}.$$

Since \tilde{T}_N is smooth in $(0, \frac{1}{N})$, the global behavior of \tilde{T}_N satisfies

$$\tilde{T}_N(I) \sim \frac{1}{N^2 \pi^2} \ln \left(\frac{1}{N \pi I} \right), \quad \forall I \in (0, \frac{1}{N}). \quad (6.13)$$

Similarly, we can compute $\tilde{T}'_N(I)$ and $\tilde{T}''_N(I)$ based on (6.7), which will involve the estimation of the complete elliptic integral of the second kind, and this leads to

$$\tilde{T}'_N(I) \sim \frac{1}{N \pi} \left(\frac{\frac{1}{2N} - I}{I} \right) \quad \text{and} \quad \tilde{T}''_N(I) \sim \frac{1}{(N \pi I)^2} \quad (6.14)$$

for all $I \in (0, \frac{1}{N})$. Using (6.13)-(6.14), we get

$$\left| \frac{\tilde{T}_N^2(I) g_N(I)}{\tilde{T}'_N(I)} \right| \leq C \frac{1}{N^3} (1 + \ln |I|^3) I, \quad (6.15)$$

$$\left\| \left(\frac{\tilde{T}_N^2 g_N}{\tilde{T}'_N} \right)' \right\|_{L^1(\delta_h, \frac{1}{2N} - \delta_e)} \leq C \frac{1}{N^4} |\ln(N \delta_e)|, \quad (6.16)$$

$$\left\| \frac{\tilde{T}_N^2(I) g^{1/2}(I)}{\tilde{T}'_N(I)} \right\|_{L^2(\delta_h, \frac{1}{2N} - \delta_e)} \leq C \frac{1}{N^3} \ln |\delta_e|, \quad (6.17)$$

and

$$\|g^{-1/2}\|_{L^2}^2 \leq C |\ln(N \delta_e)|. \quad (6.18)$$

For $\delta_e > 0$ sufficiently small, combining (6.12) with (6.15)–(6.18) yields

$$r_N(t) \leq C |\ln(N \delta_e)|^2 \frac{1}{N^4 t}. \quad (6.19)$$

Due to page constraints, we omit the detailed computations and refer the reader to [60, Lem. 4.3, (4.17)]. With these necessary results, we now turn to the proof of Proposition 2.1. The main argument will be given for part 1), as the proof of part 2) follows an analogous procedure.

Proof of Proposition 2.1 1). The proof mirrors the procedure of [60, Thm. 3]: (i) a global estimate of the mixing rate in the region away from elliptic and hyperbolic points, and (ii) local estimates in the neighborhoods of these critical points for specialized initial data.

Let $\tilde{\Omega} \subset (0, \frac{1}{N})^2$ be an open set such that $\text{supp}(\theta(t)) \cap (0, \frac{1}{N})^2 \subset \tilde{\Omega}$ for every $t \in \mathbb{R}$ and \mathcal{L}^2 stands for the Lebesgue measure on $(0, \frac{1}{N})^2$. Given sufficiently small $\delta_h, \delta_e \in (0, \frac{1}{2N})$, by (6.6) we have

$$\|\theta(t)\|_{(H^1(\Omega))'} = N^2 \sup_{\|\psi\|_{H^1(\Omega)} \leq 1} \int_{(0, \frac{1}{N})^2} \theta(t) \psi \, dx,$$

where

$$\begin{aligned} \sup_{\|\psi\|_{H^1} \leq 1} \int_{(0, \frac{1}{N})^2} \theta(t) \psi \, dx &= \sup_{\|\psi\|_{H^1} \leq 1} \left(\int_{\tilde{\Phi}(\mathbb{S}^1 \times (0, \delta_h))} \theta(t) \psi \, dx \right. \\ &\quad \left. + \int_{\tilde{\Phi}(\mathbb{S}^1 \times (\delta_h, \frac{1}{2N} - \delta_e))} \theta(t) \psi \, dx + \int_{\tilde{\Phi}(\mathbb{S}^1 \times (\frac{1}{2N} - \delta_e, \frac{1}{2N}))} \theta(t) \psi \, dx \right) \\ &= \sup_{\|\psi\|_{H^1} \leq 1} (I_1 + I_2 + I_3). \end{aligned} \quad (6.20)$$

We first estimate I_2 in the region away from elliptic and hyperbolic points. This yields a global mixing rate that is independent of the distribution of the initial data θ_0 . With the help of Lemma A2 and (6.19), we obtain that

$$\begin{aligned} \sup_{\|\psi\|_{H^1} \leq 1} I_2 &= \sup_{\|\psi\|_{H^1} \leq 1} \int_{\tilde{\Phi}(\mathbb{S}^1 \times (\delta_h, \frac{1}{2N} - \delta_e))} \theta(t) \psi \, dx \\ &\leq \|\theta_0\|_{H^1} (1 + \text{Lip}(\tilde{\Phi}))^2 r_N(t) \\ &\leq C \|\theta_0\|_{H^1} (1 + C(N\delta)^{-1})^2 |\ln(N \delta_e)|^2 \frac{1}{N^4 t}, \end{aligned} \quad (6.21)$$

where we used that $\text{Lip}(\tilde{\Phi}_N) \leq C(N\delta_h)^{-1}$ (see [60, Lem. 4.5]).

To estimate I_1 and I_2 for mixing in the regions near the hyperbolic and elliptic points, respectively, we consider some special initial data accordingly. First, applying $\|\theta(t)\|_{L^\infty} = \|\theta_0\|_{L^\infty}$ for any $t > 0$ (see (1.6) with $p = \infty$) and the two-dimensional Sobolev embedding $\|\psi\|_{L^p} \leq C(p)\|\psi\|_{H^1} \leq C(p)$ for any $2 < p < \infty$, we get

$$\begin{aligned} \sup_{\|\psi\|_{H^1} \leq 1} I_1 &= \int_{\tilde{\Phi}(\mathbb{S}^1 \times (0, \delta_h))} \theta(t)\psi \, dx \leq \|\theta_0\|_{L^\infty} \int_{\tilde{\Phi}(\mathbb{S}^1 \times (0, \delta_h))} |\psi| \, dx \\ &\leq C(\epsilon)\|\theta_0\|_{L^\infty} \|\psi\|_{L^{\frac{1}{\epsilon}}} \left[\mathcal{L}^2 \left(\tilde{\Phi}(\mathbb{S}^1 \times (0, \delta_h)) \cap \tilde{\Omega} \right) \right]^{1-\epsilon} \\ &\leq C(\epsilon)\|\theta_0\|_{L^\infty} \left[\mathcal{L}^2 \left(\tilde{\Phi}(\mathbb{S}^1 \times (0, \delta_h)) \cap \tilde{\Omega} \right) \right]^{1-\epsilon}, \end{aligned} \quad (6.22)$$

for any $\epsilon > 0$. Similarly, we have

$$\sup_{\|\psi\|_{H^1} \leq 1} I_3 \leq C(\epsilon)\|\theta_0\|_{L^\infty} \left[\mathcal{L}^2 \left(\tilde{\Phi} \left(\mathbb{S}^1 \times \left(\frac{1}{2N} - \delta_e, \frac{1}{2N} \right) \right) \cap \tilde{\Omega} \right) \right]^{1-\epsilon}. \quad (6.23)$$

As shown in the arguments for [60, (4.18)–(4.19), p. 84], one can always choose an appropriate initial datum θ_0 , along with a suitable subdomain $\tilde{\Omega} \subset \Omega$, such that $\tilde{\Phi}(\mathbb{S}^1 \times (0, \delta)) \cap \tilde{\Omega} = \emptyset$ and $\tilde{\Phi}(\mathbb{S}^1 \times (\frac{1}{2N} - \delta_e, \frac{1}{2N})) \cap \tilde{\Omega} = \tilde{\Phi}(\mathbb{S}^1 \times (\frac{1}{2N} - \delta_e, \frac{1}{2N}))$. Specifically, θ_0 can be chosen to have support in a small neighborhood of the elliptic point $P_e = (\frac{1}{2N}, \frac{1}{2N})$, say, within a ball $\mathcal{O}_\xi(P_e)$ of sufficiently small radius $\frac{1}{2N} \gg \xi > 0$, while remaining bounded away from the hyperbolic point. In this case, $\delta_h = \delta_h(\xi)$ depends only on ξ . As a result, we have

$$\begin{aligned} \sup_{\|\psi\|_{H^1} \leq 1} I_3 &\leq C(\epsilon)\|\theta_0\|_{L^\infty} \left[\mathcal{L}^2 \left(\tilde{\Phi} \left(\mathbb{S}^1 \times \left(\frac{1}{2N} - \delta_e, \frac{1}{2N} \right) \right) \right) \right]^{1-\epsilon} \\ &\leq C(\epsilon)\|\theta_0\|_{L^\infty} (\delta_e)^{2-2\epsilon}, \end{aligned} \quad (6.24)$$

where we used that $\mathcal{L}^2 \left(\tilde{\Phi} \left(\mathbb{S}^1 \times \left(\frac{1}{2N} - \delta_e, \frac{1}{2N} \right) \right) \right) \leq C(\delta_e)^2$ for some constant $C > 0$.

Consequently, for given $\delta_h > 0$, combining (6.20) with (6.21) and (6.23) gives

$$\begin{aligned} \|\theta(t)\|_{(H^1(\Omega))'} &= N^2 \sup_{\|\psi\|_{H^1} \leq 1} (I_2 + I_3) \\ &\leq C\|\theta_0\|_{H^1} (1 + C(N\delta_h)^{-1})^2 |\ln(N\pi\delta_e)|^2 \frac{1}{N^2 t} + C(\xi)\|\theta_0\|_{L^\infty} N^2 (\delta_e)^{2-2\epsilon}. \end{aligned} \quad (6.25)$$

To have the inequality hold for any $t > 0$, optimizing δ_e for the infimum of the right hand side of (6.25) gives

$$\|\theta(t)\|_{(H^1(\Omega))'} \leq C(\epsilon, \xi, \|\theta_0\|_{H^1}, \|\theta_0\|_{L^\infty}) \frac{1}{(N^2 t)^{1-\epsilon}}, \quad (6.26)$$

where $\epsilon > 0$ is arbitrarily small.

Analogous analysis can be used to show that if $\text{supp}(\theta_0)$ is near the hyperbolic point, using the volume estimate for $\mathcal{L}^2 \left(\tilde{\Phi}(\mathbb{S}^1 \times (0, \delta_h)) \right)$ we get

$$\sup_{\|\psi\|_{H^1} \leq 1} I_1 \leq C(\epsilon)\|\theta_0\|_{L^\infty} \left(\frac{4\delta_h}{N\pi} \left(1 + \ln \frac{4}{N\pi\delta_h} \right) \right)^{1-\epsilon}.$$

For given $\delta_e > 0$, applying the same optimization scheme in δ_h follows that

$$\|\theta(t)\|_{(H^1(\Omega))'} = N^2 \sup_{\|\psi\|_{H^1} \leq 1} (I_1 + I_2) \leq C(\epsilon, \xi, \|\theta_0\|_{H^1}, \|\theta_0\|_{L^\infty}) \frac{1}{(N^2 t)^{\frac{1}{3}-\epsilon}}. \quad (6.27)$$

Finally, combining (6.20) with (6.26)–(6.27) establishes the upper bound of $\|\theta\|_{(H^1(\Omega))'}$ as follows

$$\|\theta(t)\|_{(H^1(\Omega))'} \leq C(\epsilon, \xi, \|\theta_0\|_{H^1}, \|\theta_0\|_{L^\infty}) \frac{1}{(N^2 t)^{\frac{1}{3}-\epsilon}},$$

where $\epsilon, \xi > 0$ are small constants. It is clear that the upper bound can be lowered by increasing N , and this completes the proof of (2.2). \square

A3. Hamiltonian $H_N = \frac{1}{N\pi} \sin(N\pi x_1) \sin(N\pi x_2)$

The proof of part 2) in Proposition 2.1 for the scaled Hamiltonian $H_N = \frac{1}{N\pi} \sin(N\pi x_1) \sin(N\pi x_2)$ follows the same procedure as that of part 1). In this case, let $\tilde{T}_N(I)$ be the period of the closed orbit $\{H_N = \frac{1}{N\pi} \sin(N\pi I)\}$ passing through the point $(\frac{1}{2N}, I)$ for $I \in (0, \frac{1}{2N})$. Then it coincides with $\{\sin(N\pi x_1) \sin(N\pi x_2) = \sin(N\pi I)\}$. However, $\tilde{T}_N(I)$ becomes

$$\tilde{T}_N(I) = \frac{4}{N\pi} K(\cos(N\pi I)). \quad (6.28)$$

One can show that r_N in (6.12) now satisfies

$$r_N(t) \leq C |\ln(N\delta_\epsilon)|^2 \frac{1}{N^{7/2}t}, \quad (6.29)$$

and the volume estimates in I_1 and I_3 remain the same. Using the analogous optimization schemes establishes (2.3). This completes the proof of Proposition 2.1.

References

- [1] Y. Brenier, “The least action principle and the related concept of generalized flows for incompressible perfect fluids,” *Journal of the American Mathematical Society*, vol. 2, no. 2, pp. 225–255, 1989.
- [2] —, “The dual least action problem for an ideal, incompressible fluid,” *Archive for rational mechanics and analysis*, vol. 122, no. 4, pp. 323–351, 1993.
- [3] S. C. Sherwood, S. Bony, and J.-L. Dufresne, “Spread in model climate sensitivity traced to atmospheric convective mixing,” *Nature*, vol. 505, no. 7481, pp. 37–42, 2014.
- [4] A. D. Stroock, S. K. Dertinger, A. Ajdari, I. Mezic, H. A. Stone, and G. M. Whitesides, “Chaotic mixer for microchannels,” *Science*, vol. 295, no. 5555, pp. 647–651, 2002.
- [5] H. Aref, “Stirring by chaotic advection,” *Journal of Fluid Mechanics*, vol. 143, pp. 1–21, 1984. [Online]. Available: <https://doi.org/10.1017/S0022112084001233>
- [6] J. M. Ottino, *The Kinematics of Mixing: Stretching, Chaos, and Transport*. Cambridge: Cambridge University Press, 1989.
- [7] S. Balasuriya, “Dynamical systems techniques for enhancing microfluidic mixing,” *Journal of Micromechanics and Microengineering*, vol. 25, no. 9, p. 094005, aug 2015. [Online]. Available: <https://dx.doi.org/10.1088/0960-1317/25/9/094005>
- [8] L. Cortelezzi, A. Adrover, and M. Giona, “Feasibility, efficiency and transportability of short-horizon optimal mixing protocols,” *Journal of Fluid Mechanics*, vol. 597, pp. 199–231, 2008.
- [9] I. J. Couchman and E. C. Kerrigan, “Control of mixing in a Stokes’ fluid flow,” *Journal of Process Control*, vol. 20, no. 10, pp. 1103–1115, 2010. [Online]. Available: <https://www.sciencedirect.com/science/article/pii/S0959152410001253>
- [10] G. Crippa and C. Schulze, “Cellular mixing with bounded palenstrophy,” *Mathematical Models and Methods in Applied Sciences*, vol. 27, no. 12, pp. 2297–2320, 2017. [Online]. Available: <https://doi.org/10.1142/S0218202517500452>
- [11] M. F. Ettl and P. J. Schmid, “Mixing enhancement in binary fluids using optimised stirring strategies,” *Journal of Fluid Mechanics*, vol. 899, pp. A24, 21, 2020. [Online]. Available: <https://doi.org/10.1017/jfm.2020.448>
- [12] —, “Mixing by stirring: Optimizing shapes and strategies,” *Phys. Rev. Fluids*, vol. 7, p. 073904, Jul 2022. [Online]. Available: <https://link.aps.org/doi/10.1103/PhysRevFluids.7.073904>
- [13] J. Franjione and J. Ottino, “Symmetry concepts for the geometric analysis of mixing flows,” *Philosophical Transactions of the Royal Society of London. Series A: Physical and Engineering Sciences*, vol. 338, no. 1650, pp. 301–323, 1992.

-
- [14] O. Gubanov and L. Cortelezzi, “Towards the design of an optimal mixer,” *Journal of Fluid Mechanics*, vol. 651, pp. 27–53, 2010.
- [15] Z. Lin, J.-L. Thiffeault, and C. R. Doering, “Optimal stirring strategies for passive scalar mixing,” *Journal of Fluid Mechanics*, vol. 675, pp. 465–476, 2011.
- [16] M. Liu, F. Muzzio, and R. Peskin, “Quantification of mixing in aperiodic chaotic flows,” *Chaos, Solitons & Fractals*, vol. 4, no. 6, pp. 869–893, 1994.
- [17] E. Lunasin, Z. Lin, A. Novikov, A. Mazzucato, and C. R. Doering, “Optimal mixing and optimal stirring for fixed energy, fixed power, or fixed palenstrophy flows,” *Journal of Mathematical Physics*, vol. 53, no. 11, pp. 115 611, 15, 2012. [Online]. Available: <https://doi.org/10.1063/1.4752098>
- [18] G. Mathew, I. Mezić, S. Grivopoulos, U. Vaidya, and L. Petzold, “Optimal control of mixing in Stokes fluid flows,” *Journal of Fluid Mechanics*, vol. 580, pp. 261–281, 2007. [Online]. Available: <https://doi.org/10.1017/S0022112007005332>
- [19] A. Sharma and N. Gupte, “Control methods for problems of mixing and coherence in chaotic maps and flows,” *Pramana*, vol. 48, no. 1, pp. 231–248, Jan 1997. [Online]. Available: <https://doi.org/10.1007/BF02845632>
- [20] J.-L. Thiffeault, “Using multiscale norms to quantify mixing and transport,” *Nonlinearity*, vol. 25, no. 2, pp. R1–R44, 2012. [Online]. Available: <https://doi.org/10.1088/0951-7715/25/2/R1>
- [21] A. Vikhansky, “Control of stretching rate in time-periodic chaotic flows,” *Physics of Fluids*, vol. 14, no. 8, pp. 2752–2756, 2002. [Online]. Available: <https://doi.org/10.1063/1.1490135>
- [22] ———, “Enhancement of laminar mixing by optimal control methods,” *Chemical Engineering Science*, vol. 57, no. 14, pp. 2719–2725, 2002. [Online]. Available: <https://www.sciencedirect.com/science/article/pii/S0009250902001227>
- [23] H. Aref, “The development of chaotic advection,” *Physics of Fluids*, vol. 14, no. 4, pp. 1315–1325, 2002. [Online]. Available: <https://doi.org/10.1063/1.1458932>
- [24] D. D’Alessandro, M. Dahleh, and I. Mezic, “Control of mixing in fluid flow: A maximum entropy approach,” *IEEE Transactions on Automatic Control*, vol. 44, no. 10, pp. 1852–1863, 2002.
- [25] G. Froyland and N. Santitissadeekorn, “Optimal mixing enhancement,” *SIAM Journal on Applied Mathematics*, pp. 1444–1470, 2017.
- [26] O. Gubanov and L. Cortelezzi, “On the cost efficiency of mixing optimization,” *Journal of Fluid Mechanics*, vol. 692, pp. 112–136, 2012.
- [27] S. Ober-Blöbaum and K. Padberg-Gehle, “Multiobjective optimal control of fluid mixing.” in *PAMM: Proceedings in Applied Mathematics & Mechanics*, vol. 15, no. 1, 2015.
- [28] E. L. Paul, V. A. Atiemo-Obeng, and S. M. Kresta, *Handbook of industrial mixing*. Wiley Online Library, 2004.
- [29] A. J. S. Rodrigo, J. P. B. Mota, A. Lefèvre, and E. Saadjan, “On the optimization of mixing protocol in a certain class of three-dimensional Stokes flows,” *Physics of Fluids*, vol. 15, no. 6, pp. 1505–1516, 06 2003. [Online]. Available: <https://doi.org/10.1063/1.1572492>
- [30] Y. Wang, G. Haller, A. Banaszuk, and G. Tadmor, “Closed-loop Lagrangian separation control in a bluff body shear flow model,” *Physics of Fluids*, vol. 15, no. 8, pp. 2251–2266, 2003. [Online]. Available: <https://doi.org/10.1063/1.1588636>
- [31] M. Konishi, M. Inubushi, and S. Goto, “Fluid mixing optimization with reinforcement learning,” *Scientific Reports*, vol. 12, no. 1, p. 14268, 2022.
- [32] R. A. Mitchell and J. D. Meiss, “Designing a finite-time mixer: Optimizing stirring for two-dimensional maps,” *SIAM Journal on Applied Dynamical Systems*, vol. 16, no. 3, pp. 1514–1542, 2017.

-
- [33] G. Froyland, C. González-Tokman, and T. M. Watson, “Optimal mixing enhancement by local perturbation,” *SIAM Review*, vol. 58, no. 3, pp. 494–513, 2016. [Online]. Available: <https://doi.org/10.1137/15M1023221>
- [34] A. Balogh, O. Aamo, and M. Krstic, “Optimal mixing enhancement in 3-D pipe flow,” *IEEE Transactions on Control Systems Technology*, vol. 13, no. 1, pp. 27–41, 2005.
- [35] D. P. G. Foures, C. P. Caulfield, and P. J. Schmid, “Optimal mixing in two-dimensional plane Poiseuille flow at finite Péclet number,” *Journal of Fluid Mechanics*, vol. 748, pp. 241–277, 2014. [Online]. Available: <https://doi.org/10.1017/jfm.2014.182>
- [36] W. Hu, “Boundary control for optimal mixing by Stokes flows,” *Applied Mathematics and Optimization*, vol. 78, no. 1, pp. 201–217, 2018. [Online]. Available: <https://doi.org/10.1007/s00245-017-9404-6>
- [37] —, “An approximating control design for optimal mixing by Stokes flows,” *Applied Mathematics and Optimization*, vol. 82, no. 2, pp. 471–498, 2020. [Online]. Available: <https://doi.org/10.1007/s00245-018-9535-4>
- [38] W. Hu, C. N. Rautenberg, and X. Zheng, “Feedback control for fluid mixing via advection,” *Journal of Differential Equations*, vol. 374, pp. 126–153, 2023.
- [39] W. Hu and J. Wu, “Boundary control for optimal mixing via Navier–Stokes flows,” *SIAM Journal on Control and Optimization*, vol. 56, no. 4, pp. 2768–2801, 2018.
- [40] —, “An approximating approach for boundary control of optimal mixing via Navier–Stokes flows,” *Journal of Differential Equations*, vol. 267, no. 10, pp. 5809–5850, 2019. [Online]. Available: <https://doi.org/10.1016/j.jde.2019.06.009>
- [41] K. Koike, V. Nersesyan, M. Rissel, and M. Tucsnak, “Relaxation enhancement by controlling incompressible fluid flows,” *arXiv preprint arXiv:2506.22233*, 2025.
- [42] W. Liu, “Mixing enhancement by optimal flow advection,” *SIAM Journal on Control and Optimization*, vol. 47, no. 2, pp. 624–638, 2008. [Online]. Available: <https://doi.org/10.1137/050647888>
- [43] V. Arnold, “Sur la géométrie différentielle des groupes de lie de dimension infinie et ses applications à l’hydrodynamique des fluides parfaits,” in *Annales de l’institut Fourier*, vol. 16, no. 1, 1966, pp. 319–361.
- [44] J.-D. Benamou and Y. Brenier, “A computational fluid mechanics solution to the monge-kantorovich mass transfer problem,” *Numerische Mathematik*, vol. 84, no. 3, pp. 375–393, 2000.
- [45] M. Emerick and B. Bamieh, “Incompressible optimal transport and applications in fluid mixing,” *arXiv preprint arXiv:2504.01109*, 2025.
- [46] P. Danckwerts, “The definition and measurement of some characteristics of mixtures,” *Applied Scientific Research, Section A*, vol. 3, no. 4, pp. 279–296, 1952.
- [47] G. Mathew, I. Mezić, and L. Petzold, “A multiscale measure for mixing,” *Physica D: Nonlinear Phenomena*, vol. 211, no. 1-2, pp. 23–46, 2005.
- [48] G. Alberti, G. Crippa, and A. L. Mazzucato, “Exponential self-similar mixing by incompressible flows,” *Journal of the American Mathematical Society*, vol. 32, no. 2, pp. 445–490, 2019. [Online]. Available: <https://doi.org/10.1090/jams/913>
- [49] V. Chakravarthy and J. Ottino, “Mixing of two viscous fluids in a rectangular cavity,” *Chemical Engineering Science*, vol. 51, no. 14, pp. 3613–3622, 1996. [Online]. Available: <https://www.sciencedirect.com/science/article/pii/0009250996000073>
- [50] G. Crippa, R. Lucà, and C. Schulze, “Polynomial mixing under a certain stationary Euler flow,” *Physica D. Nonlinear Phenomena*, vol. 394, pp. 44–55, 2019. [Online]. Available: <https://doi.org/10.1016/j.physd.2019.01.009>

-
- [51] T. M. Elgindi and A. Zlatoš, “Universal mixers in all dimensions,” *Advances in Mathematics*, vol. 356, pp. 106807, 33, 2019. [Online]. Available: <https://doi.org/10.1016/j.aim.2019.106807>
- [52] Y. Yao and A. Zlatoš, “Mixing and un-mixing by incompressible flows,” *Journal of the European Mathematical Society*, vol. 19, no. 7, pp. 1911–1948, 2017. [Online]. Available: <https://doi.org/10.4171/JEMS/709>
- [53] J. Bedrossian and M. Coti Zelati, “Enhanced dissipation, hypoellipticity, and anomalous small noise inviscid limits in shear flows,” *Archive for Rational Mechanics and Analysis*, vol. 224, no. 3, pp. 1161–1204, 2017.
- [54] M. Coti Zelati, G. Crippa, G. Iyer, and A. L. Mazzucato, “Mixing in incompressible flows: transport, dissipation, and their interplay,” *Notices of the American Mathematical Society*, vol. 71, no. 5, pp. 593–604, 2024.
- [55] A. Fannjiang and G. Papanicolaou, “Convection enhanced diffusion for periodic flows,” *SIAM Journal on Applied Mathematics*, vol. 54, no. 2, pp. 333–408, 1994.
- [56] S. Heinze, “Diffusion-advection in cellular flows with large pecelet numbers,” 2001.
- [57] G. Iyer, X. Xu, and A. Zlatoš, “Convection-induced singularity suppression in the Keller-Segel and other non-linear PDEs,” *Transactions of the American Mathematical Society*, vol. 374, no. 9, pp. 6039–6058, 2021. [Online]. Available: <https://doi.org/10.1090/tran/8195>
- [58] G. Iyer and H. Zhou, “Quantifying the dissipation enhancement of cellular flows,” *SIAM Journal on Mathematical Analysis*, vol. 55, no. 6, pp. 6496–6516, 2023.
- [59] A. Novikov, G. Papanicolaou, and L. Ryzhik, “Boundary layers for cellular flows at high pécelet numbers,” *Communications on pure and applied mathematics*, vol. 58, no. 7, pp. 867–922, 2005.
- [60] E. Bruè, M. Coti Zelati, and E. Marconi, “Enhanced dissipation for two-dimensional hamiltonian flows,” *Archive for Rational Mechanics and Analysis*, vol. 248, no. 5, p. 84, 2024.
- [61] P. L. Combettes, “Perspective functions: Properties, constructions, and examples,” *Set-Valued and Variational Analysis*, vol. 26, pp. 247–264, 2018.
- [62] M. Hinze, R. Pinnau, M. Ulbrich, and S. Ulbrich, *Optimization with PDE constraints*, ser. Mathematical Modelling: Theory and Applications. Springer, New York, 2009, vol. 23.
- [63] M.-J. Lai and J. Lee, “A multivariate spline based collocation method for numerical solution of partial differential equations,” *SIAM Journal on Numerical Analysis*, vol. 60, no. 5, pp. 2405–2434, 2022.
- [64] —, “Trivariate spline collocation methods for numerical solution to 3D Monge-Ampère equation,” *J. Sci. Comput.*, vol. 95, no. 2, p. 56, 2023.
- [65] M.-J. Lai and L. L. Schumaker, *Spline functions on triangulations*. Cambridge: Cambridge University Press, 2007, no. 110.
- [66] G. Awanou, M.-J. Lai, and P. Wenston, “The multivariate spline method for scattered data fitting and numerical solutions of partial differential equations,” *Wavelets and splines: Athens*, pp. 24–74, 2005.